Reliability Evaluation of an Impedance-Source PV Microconverter

Yanfeng Shen*, Elizaveta Liivik†, Frede Blaabjerg*, Dmitri Vinnikov†, Huai Wang*, Andrii Chub†
Email: yaf@et.aau.dk, liisa.liivik@ttu.ee, fbl@et.aau.dk, dmitri.vinnikov@ieee.org, hwa@et.aau.dk, andriichub@ieee.org
*Department of Energy Technology, Aalborg University, Aalborg 9220, Denmark
†Department of Electrical Engineering and Mechatronics, Tallinn University of Technology, Tallinn 19086, Estonia

***Abstract*—The reliability of an impedance-source PV microconverter is evaluated based on the real-field mission profile. As part of a PV microinverter, the dc-dc microconverter is firstly described. Then the electro-thermal and lifetime models are built for the most reliability-critical components, i.e., the power semiconductor devices and capacitors. The finite element method (FEM) simulation is used for the thermal impedance extraction. The mission profile, i.e., the ambient temperature and solar irradiance, from Aalborg, Denmark is applied to the built electro-thermal model. Finally, the thermal loading profiles and annual wear-out damage accumulation are obtained. In addition, experimental measurements from a 300-W converter prototype are given.**

Keywords—PV; microconverter; reliability

I. INTRODUCTION

During the last decade, the solar photovoltaic (PV) energy continues to experience a significant growth tendency. One reason is due to the significantly reduced price of PV panels in the world market [1]. Another reason is the progressive evolution of PV power converters whose efficiency has been reported as high as 99% [2].

PV inverters can be classified into the centralized inverters, string inverters, and microinverters. Compared to the centralized and string inverters, microinverters features more advantages in low power applications such as module-level (maximum power point) MPP-tracking, low PV-system installation effort, easy monitoring and failure detection of the PV-system [3]-[4]. The typical lifetime of PV modules is 25 years, but the inverters typically have to be replaced every 5 to 10 years [5]. Therefore, the lifetime of inverters needs to be extended to match that of PV modules; as a result, lifetime prediction and reliability-oriented design of PV inverters under harsh operating conditions are becoming increasingly important [6]-[7].

Module-integrated converter (MIC) PV systems demand wide input voltage variations and load regulation at high DC voltage gain [8]; and thus the impedance source (IS) dc-dc converter family recently have gained a lot of attention [9]-[10]. In addition, the IS dc-dc converters possess other features, such as the immunity to shoot-through and open states, continuous input current, low inrush current, buck-boost functionality as well as high control flexibility [10]. For instance, a high-performance quasi-Z-source series resonant dc-dc converter (qZSSRC) is proposed and implemented in [11] for modular-level power electronics (MLPE) applications; thanks to the buck-boost functionality, a wide input voltage range from 10 V to 60 V is possible and high power conversion efficiency is achieved as well. Nevertheless, the reliability issue of impedance-source converters for MLPE applications is an open question.

In this context, this paper aims to investigate the reliability of an impedance-source PV microconverter based on real-field mission profiles and system-level electro-thermal models; such analysis has not been done before. The quasi-Z-source series resonant dc-dc converter [11] is chosen as it has superior performance and the potential to operate over 25 years. The microconverter is modelled in terms of the power loss, thermal impedance, lifetime and damage accumulation; the key electrical performance is validated by experiments on a 300-W prototype.

II. SYSTEM DESCRIPTION AND ELECTRO-THERMAL MODELING OF THE MICROCONVERTER

A. System Description

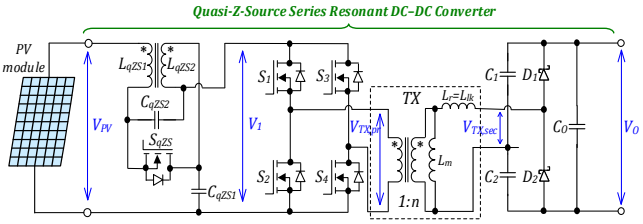

Fig. 1. Schematic of the studied PV microconverter.

The schematic of the quasi-Z-source series resonant DC/DC converter (qZSSRC) is shown in Fig. 1. As can be seen, it consists of a quasi-Z-source network, a full-bridge switching stage, an integrated series resonant tank composed of the transformer leakage inductance L_{lk} and the capacitors C_1 and C_2, voltage-doubler rectifier (VDR) diodes, and an output filter capacitor C_o. The detailed operation principle and parameter design guidelines have been presented in [11] and therefore are not repeated herein. A 300-W PV microinverter prototype, consisting of the qZSSRC, a single-phase full-bridge inverter,

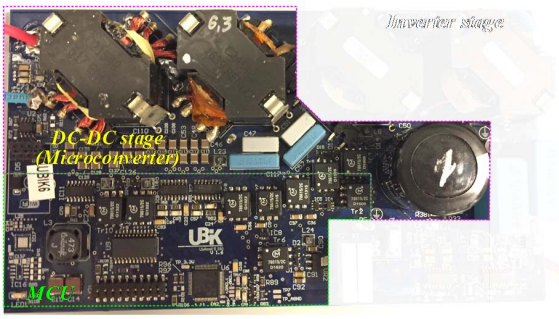

Fig. 2. Photo of the built microinverter prototype.

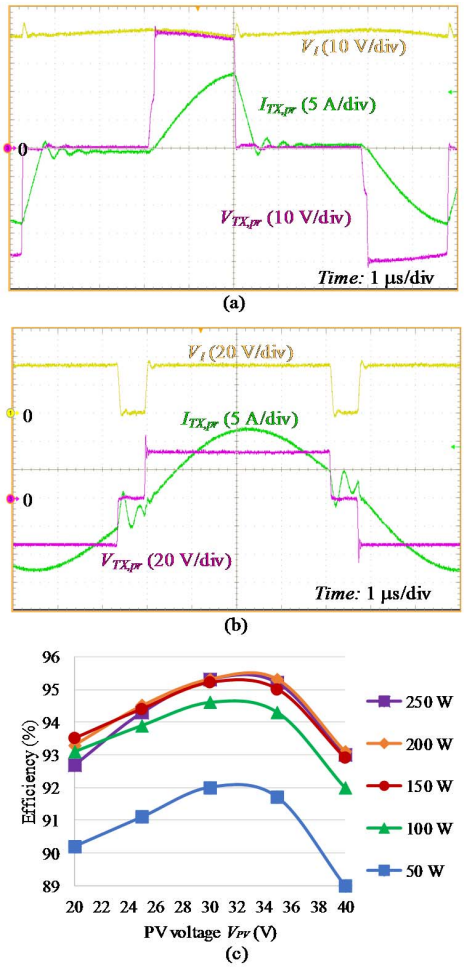

Fig. 3. Experimental waveforms in (a) Buck mode V_{PV} = 40 V and (b) Boost mode V_{PV} = 25 V; (c) measured efficiency curves (incl. the auxiliary power supply circuit).

a microcontroller unit (MCU), and an auxiliary power supply circuit, has been built and tested, as shown in Fig. 2. The detailed specifications and parameters for the qZSSRC are given in Table I. There are three operation modes: when the PV voltage $V_{PV} > 34$ V, the converter operates in the buck mode; when $V_{PV} < 34$ V, the converter operates in the boost mode; and $V_{PV} = 34$ V, the converter operates in the normal mode The measured waveforms and efficiency curves at different input power levels are given in Fig. 3.

TABLE I

SPECIFICATIONS AND PARAMETERS OF THE MICROCONVERTER PROTOTYPE

Descriptions	Parameters
Input voltage range	10-60 V
Maximum power	300 W
Rated input voltage	34 V
Most probable operating voltage range	20-40 V
Switching frequency f_s	110 kHz
Switches S_1-S_4 and S_{qZS}	BSC035N10NS5
Diodes D_1-D_2	C3D02060E
Capacitors C_{qZS1} and C_{qZS2}	2.2 µF × 12, GRM32ER72A225K
Resonant capacitors C_1 and C_2	10 nF // 33 nF, MKP1840310104M, B32672Z6333K
Output capacitor C_o	150 µF, B43501A6157M000
Transformer turns ratio n	1 : 6

B. Power Loss Modeling

In the buck mode, S_{qZS} is kept on and S_1-S_4 are soft-switched; therefore there is only conduction loss for MOSFETs. In the boost mode, S_{qZS} is turned on under ZVS (i.e., conduction loss only) whereas S_1-S_4 are hard-switched. For the rectifier diodes D_1-D_2, only the conduction loss is generated since SiC Schottky diodes are used. The conduction loss of MOSFETs can be obtain with

$$P_{T,con}(T_j) = I_{T,rms}^2 R_{ds,on}(T_j) \tag{1}$$

where $I_{T,rms}$ is the root-mean-square (RMS) current flowing through the transistor, and $R_{ds,on}$ denotes the on-state drain-source resistance which is junction temperature-dependent. Thus, the conduction loss also varies with respect to the junction temperature T_j.

The switching losses of MOSFETs are calculated with the model given in [12].

$$\begin{cases} P_{on}(T_j) = f_s V_{ds} I_{ds} \left(\dfrac{Q_{gd} R_{gon}}{V_{gs} - V_{plat}(I_{ds}, T_j)} + \dfrac{[V_{plat}(I_{ds}, T_j) - V_{th}] R_{gon} C_{iss}}{V_{gs} - V_{th}} \right) \\ P_{off}(T_j) = f_s V_{ds} I_{ds} \left(\dfrac{Q_{gd} R_{goff}}{V_{plat}(I_{ds}, T_j)} + \dfrac{[V_{plat}(I_{ds}, T_j) - V_{th}] R_{goff} C_{iss}}{V_{plat}(I_{ds}, T_j)} \right) \end{cases} \tag{2}$$

where P_{on} represents the turn-off loss, P_{off} denotes the turn-off loss, V_{ds} is the drain-source voltage applied to the MOSFET, I_{ds} is the drain-source current of MOSFET at the switching instant, R_{gon} is the turn-on gate resistance, R_{goff} is the turn-off gate resistance, Q_{gd} is the gate-drain charge, C_{iss} is the input capacitance of MOSFET, V_{plat} is the plateau value of the gate-source voltage, and V_{gs} is the amplitude of the gate-source voltage.

The conduction loss of the used SiC Schottky diodes can be expressed by

$$P_{D,con} = I_{D,avg} V_{D0} + I_{D,rms}^2 R_{D,on} \tag{3}$$

where $V_{D0} = 0.98 - 0.0011 \times T_{jD}$ and $R_{D,on} = 0.18 + 0.0018 \times T_{jD}$ [13], and T_{jD} is the junction temperature of the diode.

For the whole microinverter, the instantaneous power $p_o(t)$ contains a fluctuating power at twice the line frequency, which is decoupled by the output capacitor C_o in this converter. Thus, the electrical stresses over C_o can be calculated by [14]

$$\begin{cases} \Delta V_o \approx P_o / (\omega_0 C_o V_o) \\ I_{Co,rms} = P_o / (\sqrt{2} V_o) \end{cases} \quad (4)$$

where P_o is the average power injected to the grid, ΔV_o is the peak-to-peak ripple of the capacitor voltage V_o, and $I_{Co,rms}$ is the RMS current flowing through the output capacitor C_o.

An aluminum electrolytic capacitor can be modeled as an ideal capacitor in series with an equivalent series resistor (ESR) and an equivalent series inductor (ESL) [14]-[15]. The internal hot-spot temperature T_h is the main failure mechanism of aluminum capacitors. The power loss is mainly caused by the ripple current

$$P_{Co,loss} = I_{Co,rms}^2 \cdot ESR(T_h) \quad (5)$$

where the ESR is hot-spot temperature dependent [16]. For the ceramic and film capacitors (C_{qZS} and C_1-C_2), their power losses can be calculated in the similar way.

C. Thermal Modeling

The PV microconverter is built with a four-layer PCB and is enclosed in an aluminum case (200 mm × 150 mm× 45 mm) with natural convection. System-level FEM simulations are conducted to extract the thermal resistances for the components in the PV microconverter. The structure models of main components, enclosure and PCB used in FEM simulations are shown in Fig. 4. With the FEM simulation results, each junction/hotspot-to-ambient thermal impedance $Z_{ja}(t)$ can be fitted as a Kth-order Foster model, i.e.,

$$Z_{ja}(t) = \sum_{k=1}^{K} R_{ja,k}(1 - e^{-t/\tau_{ja,k}}) \quad (6)$$

where $R_{ja,k}$ is the junction/hotspot-to-ambient thermal resistance (i.e., the steady-state value of the junction/hotspot-to-ambient thermal impedance $Z_{ja}(t)$), and the time constant $\tau_{ja,k} = R_{ja,k} C_{ja,k}$, with $C_{ja,k}$ being the junction-to-ambient thermal capacitance.

Then, the junction/hotspot temperature can be obtained by

$$T_j(t) = T_a + \int_0^t P_l(\tau) dZ_{thja}(t - \tau) d\tau \quad (7)$$

D. Lifetime Modeling

The lifetime of power semiconductor devices mainly depends on the junction temperature, i.e., mean junction temperature T_{jm}, temperature swing ΔT_j and heating time t_{on}. In this paper, an empirical lifetime model— Bayerer's model [17] is used

$$N_f = A \cdot (\Delta T_j)^{\beta_1} \cdot \exp\left(\frac{\beta_2}{T_{jm} + 273}\right) \cdot t_{on}^{\beta_3} \quad (8)$$

where A, β_1, β_2 and $\beta_1$are fitting parameters obtained from the test data of device manufacturer, and N_f is the number of cycles to failure under the specific thermal stress of T_{jm}, ΔT_j and t_{on}.

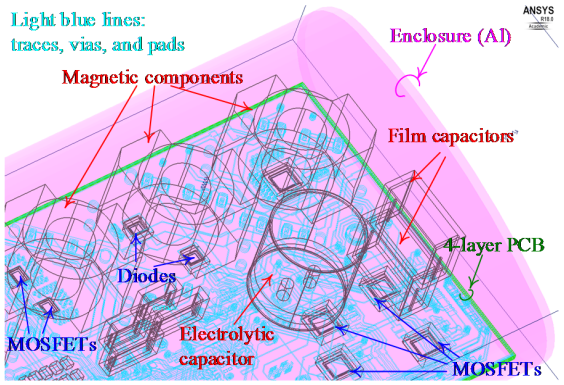

Fig. 4. Structure models of main components, enclosure and PCB used in FEM simulations.

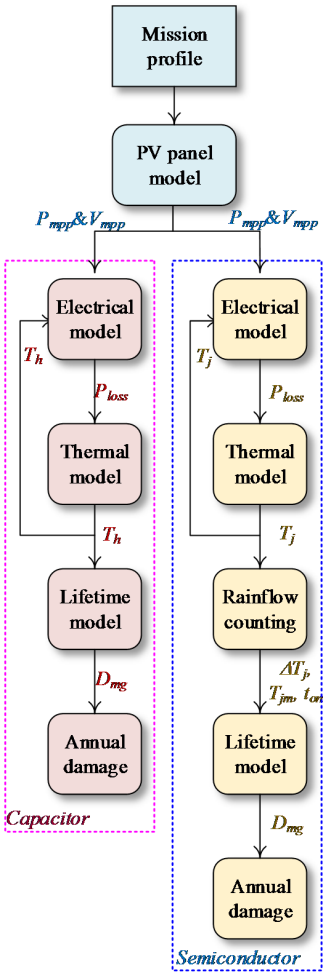

Fig. 5. Flowchart of reliability evaluation for the PV microconverter.

The rain-flow counting algorithm is adopted to extract the number of thermal cycles with the specific T_{jm}, ΔT_j, and t_{on} [18].

A widely-used capacitor lifetime model is employed for the lifespan projection of capacitors [19]-[20]

$$L_{cn} = L_{c0} \cdot 2^{\frac{T_0 - T_h}{n_1}} (V / V_0)^{-n_2} \quad (9)$$

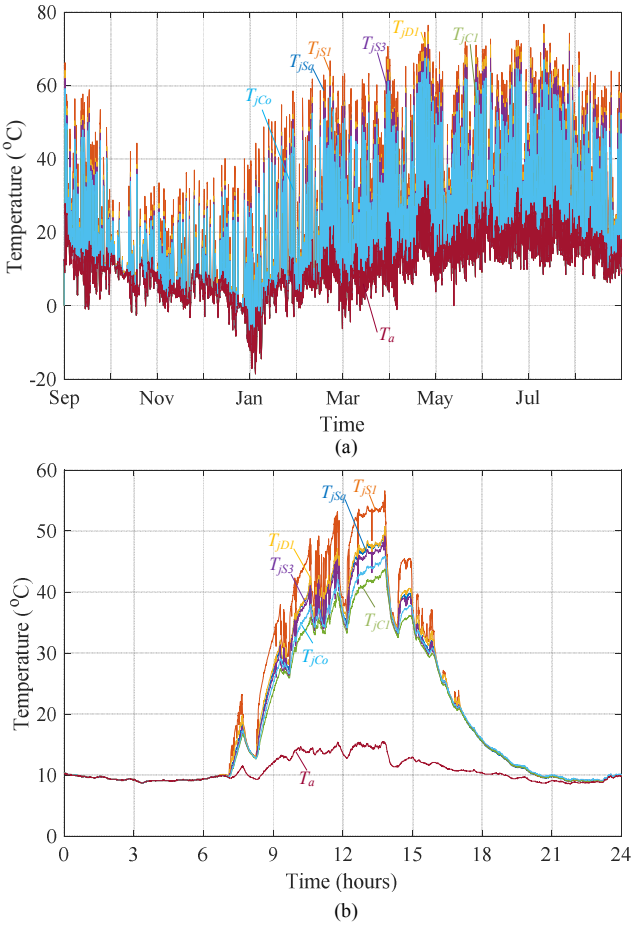

Fig. 6. (a) Long-term (one-year) and (b) short-term (one-day) power loss and junction temperature profiles for different components when the microconverter operates in Aalborg, Denmark.

in which L_{cn} is the lifetime under the thermal and electrical stress T_h and V, L_{c0} is the lifetime under the reference temperature T_0 and the nominal voltage V_0. The coefficient n_1 is a temperature dependence constant, and n_2 is the voltage stress exponent. For small-size radial type capacitors, when the applied voltage is below the rated voltage, the temperature-dependent electrolyte loss is the dominant failure mechanism, and thus n_2 is equal to 0 [21]. The exponent n_2 is from round 7 to 9.4 for film capacitors [19]. For the ceramic capacitor used in this prototype, the manufacturer provides the coefficients n_1 = 8, and n_2 = 3 [22].

As for the damage accumulation, the commonly used Miner's rule [23] which assumes the damage accumulates linearly , is employed in this paper, i.e.,

$$D_{mg} = \sum_k (n_k / N_{fk}) \tag{10}$$

where n_k is the number of temperature cycles corresponding to the specific combination of T_{jm}, ΔT_j and t_{on}, and N_{fk} is the number of cycles to failure for the same thermal loading stress. It is assumed that the device fails when D_{mg} is accumulated to 1.

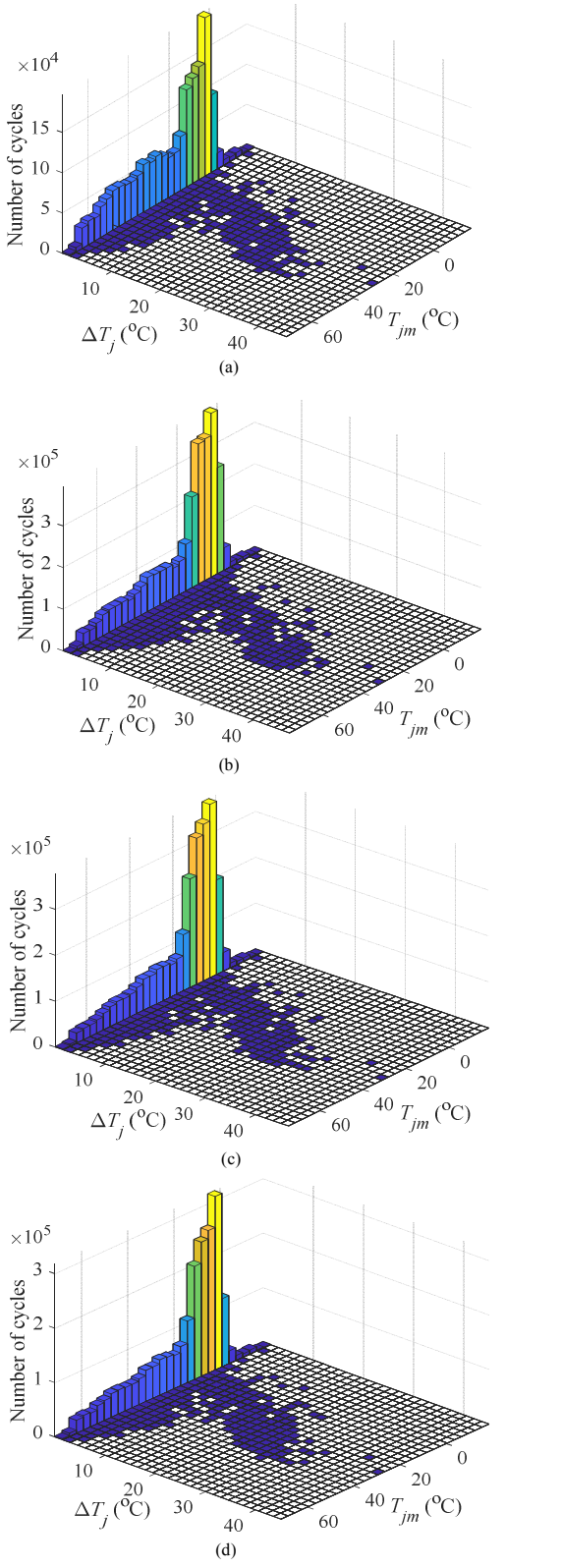

Fig. 7. 3-D histograms of rain-flow counting results of one-year junction temperature profiles for different power semiconductor devices: (a) S_{qZS}, (b) S_1, (c) S_3 and (d) D_1.

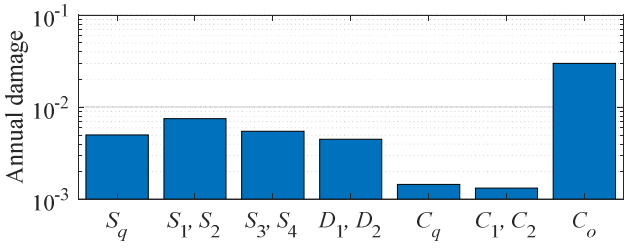

Fig. 8. Annual wear-out damages for critical components.

III. Reliability Evaluation of the Microconverter

The flowchart of reliability evaluation for the PV microconverter is shown in Fig. 5. With the PV panel model and the maximum power point tracking (MPPT) control, the long-term mission profile can be translated into the real-time voltage and power at the maximum power point, V_{mpp} and P_{mpp}, which are the input of the microinverter. The power loss and junction/hotspot temperature of a component can be subsequently calculated based the power loss model and the thermal model, as shown in Fig. 6. As mentioned before, the rain-flow counting algorithm is employed to extract the number of temperature cycles with different characteristics (e.g., the mean temperature T_{jm}, temperature swing ΔT_j and heat-on time t_{on}), as illustrated in Fig.7. After that, the lifetime model and damage accumulation model (e.g., Miner's rule) is used to estimate the accumulated damage over a year. It is worth noting that the junction/hotspot temperature T_j also affects the power loss, which is taken into account herein. When the damage is accumulated to 1, it is assumed that the component fails. Thus components' lifetimes due to wear out can be derived.

Fig. 8 depicts the annual wear-out damage for each critical component. It can be seen that the dc-link electrolytic capacitor has the highest wear-out damage accumulation over a year, i.e., about 0.03, which means that the accumulated wear-out damage can be as high as 0.6 after 20-year operation.

IV. Conclusions

The reliability of the quasi-source series resonant dc-dc converter (as the dc-dc stage of a 300-W PV microinverter) is evaluated based on the mission profile at Aalborg, Denmark. The system operation and implementation are introduced; then the electro-thermal models (including the power loss and thermal models) and lifetime models are built for critical components. Finally, the annual damage data is obtained for each component. It reveals that the dc-link electrolytic capacitor accumulates the highest damage each year, and may have the shortest lifetime due to wear out.

References

[1] L. Tinker and R. Jones-Albertus, "Emerging PV technologies: The path to market competitiveness," *2016 IEEE 43rd Photovoltaic Specialists Conference (PVSC)*, Portland, OR, 2016, pp. 3471-3474.

[2] R. M. Burkart and J. W. Kolar, "Comparative Life Cycle Cost Analysis of Si and SiC PV Converter Systems Based on Advanced η-ρ-σ Multiobjective Optimization Techniques," *IEEE Transactions on Power Electronics*, vol. 32, no. 6, pp. 4344-4358, June 2017.

[3] H. Oldenkamp and I. de Jong, "The return of the ac-module inverter," *in Proc. 24th Eur. Conf. Photovolt. Solar Energy*, Hamburg, Germany, Sep. 2009, pp. 3101–3104.

[4] S. B. Kjaer, J. K. Pedersen, and F. Blaabjerg, "A review of single phase grid-connected inverters for photovoltaic modules," *IEEE Trans. Ind. Appl.*, vol. 41, no. 5, pp. 1292–1306, Oct. 2005.

[5] M. A. Maehlum, "*The Real Lifespan of Solar Panels*," available online [2017], http://energyinformative.org/lifespan-solar-panels/.

[6] B. Gu, "Power converter and control design for high-efficiency electrolyte-free microinverters," Ph.D dissertation, Blacksburg, VA, Nov. 2013.

[7] H. Wang et al., "Transitioning to Physics-of-Failure as a Reliability Driver in Power Electronics," *IEEE Journal of Emerging and Selected Topics in Power Electronics*, vol. 2, no. 1, pp. 97-114, March 2014.

[8] S. Kouro, J.L. Leon, D. Vinnikov, L.G-. Franquelo, "Grid-Connected Photovoltaic Systems: An Overview of Recent Research and Emerging PV Converter Technology," *IEEE Industrial Electronics Magazine*, vol.9, no.1, pp.47-61, Mar. 2015

[9] A. Chub, D. Vinnikov, F. Blaabjerg, and F.Z. Peng, "A Review of Galvanically Isolated Impedance-Source DC–DC Converters," *IEEE Trans. Power Electron.*, vol. 31, no. 4, pp. 2808-2828, Apr. 2016.

[10] Y. P. Siwakoti, F. Z. Peng, F. Blaabjerg *et al.*, "Impedance-Source Networks for Electric Power Conversion Part I: A Topological Review," *IEEE Trans. Power Electron.*, vol. 30, no. 2, pp. 699-716, Feb. 2015.

[11] D. Vinnikov, A. Chub, L. Liivik, and I. Roasto, "High-performance quasi-Z-source series resonant DC-DC converter for photovoltaic module level power electronics applications," *IEEE Trans. Power Electron*., vol. 32, no. 5, pp. 3634-3650, May 2017.

[12] A. Lidow, J. Strydom, M. d. Rooij, and D. Reusch, *GaN Transistors for Efficient Power Conversion*, 2nd ed. Efficient Power Conversion Corporation: Wiley Press, 2015.

[13] Datasheet: C4D02120E SiC Schottky Diode, available online [2017]: http://www.wolfspeed.com/media/downloads/128/C4D02120E.pdf

[14] H. Wang, Y. Yang, and F. Blaabjerg, "Reliability-oriented design and analysis of input capacitors in single-phase transformer-less photovoltaic inverters," *in Proc. of APEC'13*, pp. 2929-2933, Mar. 2013.

[15] Y. Shen, H. Wang, and F. Blaabjerg, "Reliability Oriented Design of a Grid-Connected Photovoltaic Microinverter," *in Proc. IFEEC-ECCE Asia 2017*, pp. 1-6, Jun. 2017.

[16] "General description of aluminum electrolytic capacitors", available online [2017]: http://www.nichicon.co.jp/english/products/pdf/aluminum.pdf.

[17] R. Bayerer, T. Herrmann, T. Licht, J. Lutz, and M. Feller, "Model for power cycling lifetime of IGBT modules - various factors influencing lifetime," *in Proc. of Integrated Power Systems (CIPS) 2008*, pp.1-6, 2008.

[18] K. M. Matsuishi and T. Endo, "Fatigue of metals subjected to varying stress," *Jap Soc. Mech. Eng*., pp. 37-40, Mar. 1968.

[19] H. Wang, and F. Blaabjerg, "Reliability of capacitors for DClink applications in power electronic converters—an overview," *IEEE Trans. on Industry Applications*, vol. 50, no. 5, pp. 3569-3578, Sep. 2014.

[20] A. Albertsen, "*Electrolytic capacitor lifetime estimation*," available online [2017]: http://www.jianghai-america.com

[21] D. Zhou, H. Wang, and F. Blaabjerg, "Lifetime estimation of electrolytic capacitors in a fuel cell power converter at various confidence levels," *in Proc. of SPEC 2016*, pp. 1-6, 2016.

[22] muRata, "Ceramic Capacitors FAQ," Available online [2017] http://www.murata.com/support/faqs/products/capacitor/mlcc/qlty/0010

[23] M. F. Ashby and D. R. H. Jones, Engineering Materials 1—An Introduction to Properties, Applications and Design, 3rd ed. Oxford, U.K: Butterworth–Heinemann.